Geomorphology 403 (2022) 108180

Contents lists available at ScienceDirect

Geomorphology

journal homepage: www.journals.elsevier.com/geomorphology

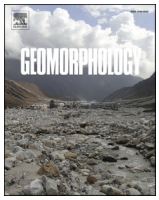

Assessing functional characteristics of a braided river in the Qinghai-Tibet Plateau, China

Peng Gao [a,*], Zhiwei Li [b,*], Yuchi You [c], Yinjun Zhou [d], Hervé Piégay [e]

[a] Department of Geography and the Environment, Syracuse University, Syracuse, NY 13244, USA
[b] State Key Laboratory of Water Resources and Hydropower Engineering Science, Wuhan University, Wuhan 430072, China
[c] School of Hydraulic and Environmental Engineering, Changsha University of Science & Technology, Changsha 410114, China
[d] Changjiang River Scientific Research Institute, Wuhan 430010, China
[e] University of Lyon, UMR 5600 CNRS – EVS, Site of ENS, 15 Parvis R. Descartes, F-69362 Lyon, France

ARTICLE INFO

Keywords:
High-elevation braided river
Flowing channel
Active channel width
Braiding intensity
Bar vegetation

ABSTRACT

Functional characteristics of braided rivers with very high elevations (>3400 m) located in the Qinghai-Tibet Plateau, China provide unique insight into fully understanding global braided river functioning, but have not yet been explored because of their remote locations and harsh physiographic conditions. In this study, we unveiled these characteristics at the reach spatial scale over three decades in one of these braided rivers, the Upper Lancang River (ULR). Using Google Earth Engine resources and a specific selection of Landsat images obtained between 1989 and 2018 during the dry season (November to early May when water levels were low and comparable over years), we analyzed water area, extracted flowing and non-flowing channels, active channel widths (unvegetated bars and water channels), and calculated lateral shifting rates of the main channel for 13 subperiods. We also developed an empirical method for estimating vegetated areas in the selected years. We found that (1) this braided system is partly controlled by peak flows and flood durations and the braiding activity evolved through time according to braided planform characteristics, (2) braiding intensity is high during low discharges, suggesting that the ULR is a very well-connected braided system with groundwater, but we observed higher braiding activity in spring than in fall, suggesting other factors than groundwater recharge also control non-flowing channel occurrence, and (3) the ULR supports a vegetation mosaic that is dynamic at a multi-year scale with period of declines that can be caused by scouring and rapid growth in an optimal recruitment window. These findings lead to our interpretation of vegetation behavior and surficial water – groundwater interactions, which needs future field validation.

1. Introduction

As indicated by Elosegi et al. (2010), geomorphology provides an integrative and systemic framework to understand river functioning that affects river biodiversity. "Functioning" refers to a set of processes and interactions that sustain a river as a system. It can be either physical (hydrological, geomorphological), chemical, or biological (Jax, 2005). Along this line, functions are the roles played by a river system in providing diverse habitats (e.g., channel shifting, upwelling and downwelling processes, and structural effects of vegetation). Thus, morphodynamics are critical controls of river functioning, which may be embodied as rivers being either responsive/sensitive to change, or resilient. River functioning can also be characterized by specific interactions between surface and subsurface flow compartments or vegetation processes that influence channel morphodynamics (Gurnell, 2014). Among existing river planform types on Earth, braided rivers have one of the most complex biomorphologic structures that lead to more dynamic river functions (Malard, 2003; Tockner et al., 2006). Braided rivers are considered as mountain rivers, as their functions are primarily available in mountain environments (Ward et al., 1999). Nevertheless, many braided rivers still do not share these specific functions because of highly diverse valley settings, sediment supply and vegetation dynamics. Indeed, braided rivers can provide a range of ecological functions depending on their specific functioning (see discussion in Belletti et al., 2013).

The generally complex morphology of braided rivers results from

* Corresponding authors.
E-mail addresses: pegao@syr.edu (P. Gao), lizw2003@whu.edu.cn (Z. Li).

https://doi.org/10.1016/j.geomorph.2022.108180
Received 20 November 2021; Received in revised form 17 February 2022; Accepted 18 February 2022
Available online 23 February 2022
0169-555X/© 2022 Elsevier B.V. All rights reserved.

interaction among flows, sediment delivery, and vegetation. This interaction is mainly driven by (1) flood regime and sediment transport (Bertoldi et al., 2009; Camporeale et al., 2013; Egozi and Ashmore, 2009; Gurnell et al., 2012) and (2) hydroclimatic conditions that influence vegetation dynamics (Tal et al., 2004; Gurnell et al., 2012; Belletti et al., 2015). Existing field-based studies on morphodynamic processes of braided rivers have shown that river functioning is often site-specific because of the complex interactions between different drivers (Bertoldi et al., 2013; Carley et al., 2012; Schwenk et al., 2017; Williams et al., 2015). Therefore, directly predicting spatially and temporally variable functions of braided rivers using existing findings is difficult (Ashmore, 2013; Bertoldi et al., 2009; Williams et al., 2016). A pressing need exists for more research on natural braided rivers in different regions of the world that will ultimately help develop complete theories on braiding functions (Ashmore, 2013) with an improved temporal resolution.

Thus far, almost all studies on braided characteristics and changes of natural braided rivers, with the aid of emerging techniques such as terrestrial laser scanner and unmanned aerial vehicle (UAV), have focused on various temperate, alpine, and cold zones (Cucchiaro et al., 2019; Horn et al., 2012; Huber and Huggenberger, 2015; Javernick et al., 2014; Kasai et al., 2019; Leduc et al., 2015; Lotsari et al., 2018; Middleton et al., 2019; Picco et al., 2013; Tamminga et al., 2015; Williams et al., 2015). In addition, studies of the link between the morphology of braided networks and its biophysical characteristics have been limited primarily to a few European braided rivers (Belletti et al., 2013; Belletti et al., 2015; Wawrzyniak et al., 2013). Very little is known about functioning characteristics of braided gravel-bed rivers in the Qinghai-Tibet Plateau of western China.

These rivers have developed in alluvial valleys with elevations above 3500 m and typically extend over 1 km laterally (Li et al., 2020). Controlled by the unique alpine monsoon climate that features a long, cold, dry season, their morphological structures respond to the dominant hydrological regimes. Exploring whether these responses are similar to those in other regions would provide valuable scientific insights into our knowledge of key factors controlling braided rivers in general. The Upper Lancang River (ULR) is one of these rivers that is of particular importance because of its unknown impact on the downstream basin in Southeast Asia, conventionally referred to as the Lower Mekong River basin where sediment dynamics and its response to potential cascade dams have been thoroughly studied (Grumbine et al., 2012; Kummu et al., 2010; Lu et al., 2014).

Nonetheless, the harsh physical setting and remote location of the ULR make in situ measurements very difficult. As such, data scarcity is a serious challenge for deciphering historical changes and braided river behaviors in the ULR, an issue not encountered in many other regions (Bertoldi et al., 2011; Cienciala and Pasternack, 2017; Middleton et al., 2019). In particular, it is challenging to obtain information on (i) channel shifting and braided planform changes; (ii) interactions between groundwater and surface runoff (potentially very important for understanding habitat patterns in the braided river system) (Belletti et al., 2013; Malard et al., 2006), and (iii) vegetation recruitment, growth and scouring, which is largely unknown in such high-altitude environment. These difficulties are because the existing methods for examining the characteristics of river vegetation or the above-mentioned interactions largely rely on second-hand survey data and higher resolution optical images, such as airborne LiDAR, aerial, or multispectral images and Unmanned Aerial Vehicle (UAV) photos (Hugue et al., 2016; Lallias-Tacon et al., 2017; Naura et al., 2016; Sanhueza et al., 2019; Solari et al., 2015). These data are not available for braided rivers in the ULR and other remote regions. Discharge series, especially, peak flow series, are also very limited. Nonetheless, they are central for explaining behavior of braided rivers through time (Belletti et al., 2013; Lallias-Tacon et al., 2017; Malard et al., 2006). The general data shortage explains why no study has ever been conducted on functioning characteristics of ULR braided rivers.

Within this context, we argue that because the ULR rivers are fairly wide (more than 1 km), it is possible to take advantage of existing Landsat data available since 1984 and accessible with the Google Earth Engine interface for exploring temporally variable functions of these rivers. We hypothesize that combining a sufficiently long time series of Landsat images with limited hydrological data and high-resolution images can offer a new approach to reveal temporal patterns of the morphodynamics of these rivers. This study tests this hypothesis by effectively coupling limited hydrological data with UAV data, and Landsat and Google Earth images to reveal key functional characteristics of a braided reach within the selected ULR reach including (1) multi-decadal planform change and channel shifting; (2) surface and subsurface flow interactions from aquatic patches at low flows and (3) associated vegetation dynamics in the braidplain of the reach.

2. Material and methods

2.1. Study area

The Upper Lancang River (ULR) region is situated in the eastern Qinghai-Tibet Plateau of China. It is bounded by the Yangtze River source area in the north and the Nujiang River source area in the south (Fig. 1a). Geologically, the ULR region belongs to the Gangdese Block, one of the structural blocks formed by collision between the Indus Plate and Eurasian Continent. Thus, the region has witnessed long-term sedimentation that was subsequently turned into red sandstone that is easily shaped by fluvial forces. Geomorphologically, the ULR region features mountains several thousand meters high and valleys with elevations ranging approximately between 3400 and 3700 m. Therefore, braided rivers occupying the alluvial parts of valleys are highland rivers accompanied by alpine meadows, wetlands, and trees.

The ULR region is dominated by a typical monsoon climate with distinct wet (June–October) and dry (November–May) seasons. Consequently, annual precipitation mainly occurs during summer months. From 1960 to 2017, mean annual precipitation (P) remained around 549.9 mm with very small variations (coefficient of variation, CV = 0.154), though annual mean temperature (T) has increased gradually at an accelerated rate after 1997 (Fig. 2a). The two trends indicate that a continuous increase of temperature has not caused a perceptible increase of precipitation in the past five decades. Annual mean discharge (Q_m) stayed around 139.4 m^3/s with a small range of variation (CV = 0.210). The mean runoff coefficient was 0.482 with CV = 0.158. These results signified that the flow regime in the ULR has remained relatively stable for decades, though global climate change has apparently caused a continuous increase of T. For each year with daily discharge data, high flows always emerged during summer (i.e., from June to September) and peak discharges (Q_{peak}) tended to occur between late June and middle August (Fig. 2b). From November to early May, discharges were low and varied less, but generally showed higher magnitudes in the October–December period than those in the January–early May period.

In this study, we focused on a braided reach of the ULR located near Nangqian County (33°45′48″ N, 94°40′52″ E), Yushu Tibetan Autonomous Prefecture of Qinghai Province, China (Fig. 1b). This reach has an average elevation of around 3500 m and a drainage area of about 16,434 km^2. It is approximately 6 km long and has a mean channel slope of about 1.57‰ (Fig. 1c). The widest valley width is about 1.2 km near the middle of the reach. Although the narrowest valley ~600 m wide in the downstream section is confined by mountains on both sides, almost all channel branches still have rooms for lateral migration. River beds and bars between braided channels are predominantly comprised of gravels with the mean sizes ranging between about 0.03 and 0.04 m. Willow trees and shrubs, mixed with herbs grow on the gravel bars and their densities vary spatially. Grass is also distributed on portions of many gravel bars topped by sand and silts. Physiographic features of braided channels and the bars that divide them vary in the longitudinal direction of the studied reach, which may be discernable from a series of images obtained using a lightweight unmanned aerial vehicle (UAV)

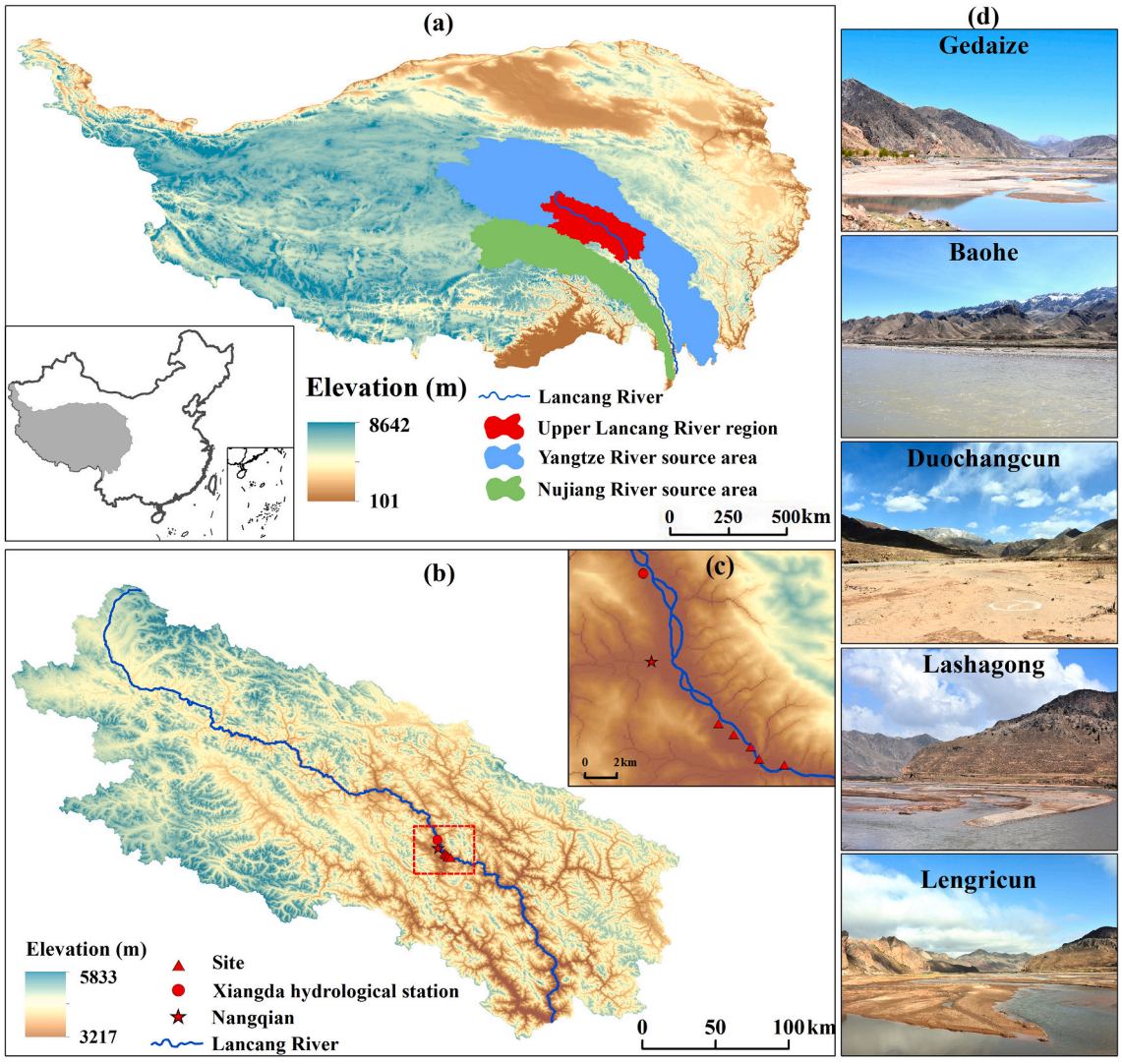

Fig. 1. The studied braided reach in the Upper Lancang River (ULR) region and its physical environment. (a) Geographic and geomorphological settings of the ULR region in the Qinghai-Tibet Plateau, China; (b) The specific location of the studied braided reach in the ULR region; (c) The studied braided reach and the relative positions of the gauging station, the Nangqian county, and five survey sites; and (d) Pictures of the five sub-zones surveyed by a UAV from upstream to downstream.

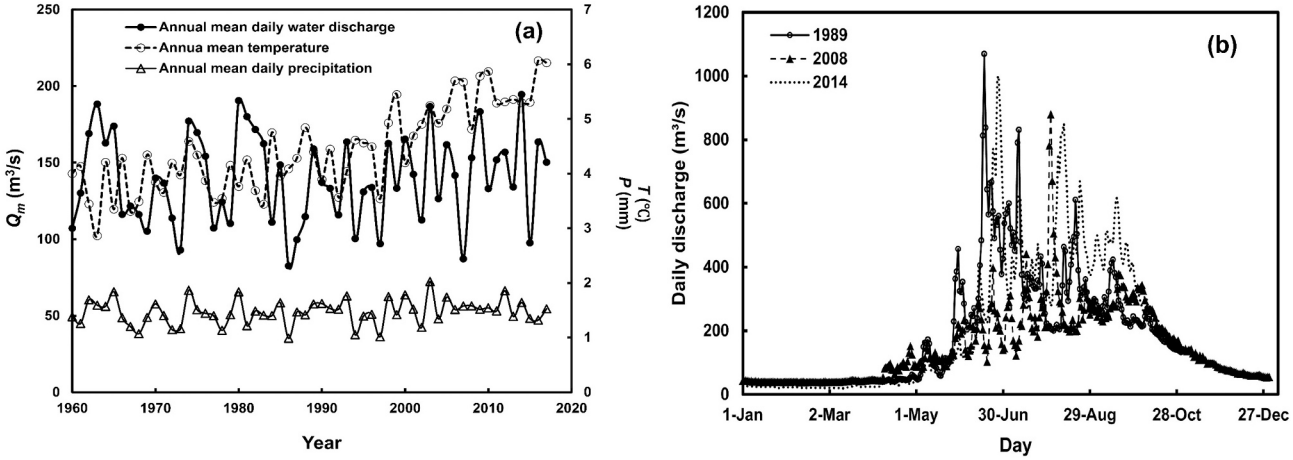

Fig. 2. Climate conditions and the hydrological regime of the studied region. (a) Decadal changes of annual mean discharge, temperature, and precipitation; (b) Seasonal changes of daily discharges in three selected years.

along the studied braided reach from upstream to downstream (Fig. 1d).

The upstream section of the study reach has already been affected by a set of anthropogenic pressures: (1) The city of Nangqiann located about 4 km upstream of this reach embanked a section over a length of about 6.6 km in 2017; (2) A large gravel mining area with active urban development is also observed immediately downstream of this section, partially offsetting the potential impact of embankment on sediment delivery downstream; (3) a small upstream dam diverting water for irrigation was built in 1989.

2.2. Data acquisition and pre-processing

We first obtained online data as a single polygon for the studied reach from Global Surface Water (https://global-surface-water.appspot.com/map) and used the climate engine interface to explore variability of NDWI (Normalized Difference Water Index) and NDVI (Normalized Difference Vegetation Index) over the whole period for which data are available (i.e., 1984–2018) (https://app.climateengine.org/climateEngine) (Fig. 3).

A set of Landsat images (30 m resolution) spanning from 1988 to 2018 were downloaded from Computer Network Information Center, Chinese Academy of Sciences (http://www.gscloud.cn) and US Geological Survey (https://earthexplorer.usgs.gov/). Image selection was guided by two principles. First, images covering the studied reach should be clear with no discernable cloud cover, such that the morphological structure of the reach may be extracted. Second, and more importantly, images must be taken during the cold, dry season, which extends approximately from November to early May during each hydrological year. So little precipitation occurs in the dry season that river flows in the studied braided reach are generally base flows (Fig. 2b). Therefore, satellite images obtained during this period assured that (1) braided channels and gravel bars were most exposed to be defined on the images, and (2) variations of water levels over the study period were constrained to better investigate groundwater – surficial water interactions. Based on these two rules and the availability of images, we selected 20 images between 1988 and 2018 (see Supplementary materials, Table S1). In addition, we selected 3–6 images within each year of the five years (1992, 2008, 2013, 2014, 2017) over a gradient of daily discharge from 50 to 250–300 m^3/s for characterizing seasonal changes of flowing channel patterns. These images have already been pre-processed to Level 1T (Standard Terrain Correction) as GeoTIFF files with the UTM-WGS84 coordinate system. Each original image was further pre-processed for radiance calibration and atmosphere correction.

Limited hydrological and meteorological data are available in a gauging station (Xiangda) maintained by Changjiang Hydrological Bureau of China. These data (Fig. 2) included (1) daily mean temperature, daily mean precipitation (P_m), annual mean discharges (Q_m) from 1960 to 2017 (missing data in the 1993–2006 period), and (2) daily mean (Q_{daily}) and annual peak (Q_{peak}) discharges for 13 yr (Table S1). By establishing the relationship between P_m and Q_m, which was strong and statistically significant, we estimated Q_m values in the missing period using obtained P_m values. Given that the station is located about 10.6 km upstream of the studied braided reach (Fig. 1c), these data should be converted to discharges passing through the studied braided reach. The conversion was achieved using the classic linear scaling method (McCuen, 2004) based on the two contributing areas to the gauging station and the input point of the study reach. Flood frequency analysis, based on the available peak discharges in eleven hydrological years, showed that discharges with one (Q_1), two (Q_2), and five (Q_5) year return intervals are 440, 603.3, and 837.8 m^3/s, respectively. The years with measured daily discharges do not match those with available images (Table S1), which greatly hindered the potential to link morphological changes of the studied braided reach to the associated hydrological variations. To increase this potential, online data provided by the climate engine interface (e.g., surface water area based on NDWI) were subsequently used to indirectly retrieve some discharge information in some of the years without measured discharge data (Table S1).

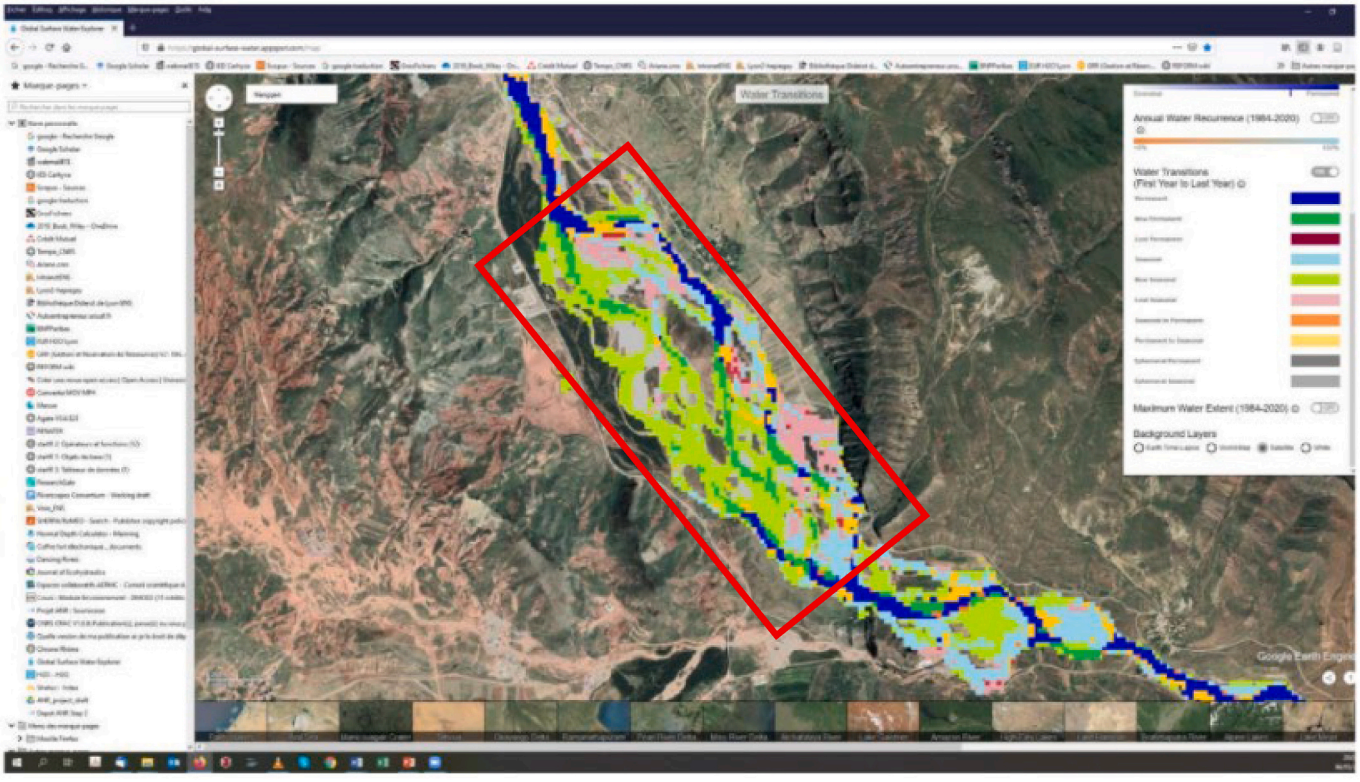

Fig. 3. Example of mean daily NDWI values calculated within the study reach marked by a red rectangle.

From May 17–19, 2018, the studied braided reach was surveyed using a lightweight UAV (DJI Phantom 4 Advanced). that flew about 160 m above the ground at an average velocity of about 9.2 m/s. The overlap of the images was set at 80% to assure a very high resolution. On the survey days, the sky was clear and the wind speed was less than 2 m/s, which allowed us to obtain clear pictures. Five sub-zones with variable areas and extents were surveyed from the upstream to the downstream extent of the reach (Fig. 1c). The UAV images were subsequently processed using a combination of several software packages (i.e., Pix4D, Cloud Compare, and ArcGIS) based on Structure-from-Motion photogrammetry, which led to five high-resolution ortho-images representing five segments (Fig. 4a–e). These images were then converted into a high-resolution DEM (0.3 m planar resolution). The error was determined by comparing an independent set of elevation data obtained using an RTK GPS with the associated points identified from the UAV data. The result showed that the vertical resolution of the DEM was 0.08 ± 0.03 m. The ortho-images were then used for both extracting channels and supervising classification of a vegetation index and estimating vegetation areas in all pixels of the selected Landsat images. The DEM was used for accuracy assessment of the Landsat images.

2.3. Methods of analysis

2.3.1. Assessing daily discharges in years with no measured data

The downloaded 31 images in which the water surface area is observable based on NDWI threshold values spanned from 1984 to 2018. The downloaded mean daily NDWI values were observed from the studied braided reach over the period 1980–2020. These mean daily NDWI values in the 13 yr with measured Q_{daily} values (Table S1) were isolated and examined in detail. In winter months of some years, mean daily NDWI values representing surface water were abnormally high (Fig. 5a). Comparing the Landsat images for these days against those in similar times, but having normal mean daily NDWI values, showed that the former images were covered by snow or ice, which skewed the obtained mean daily NDWI values (see Supplementary Fig. S1). We then compared normal mean daily NDWI values with the associated daily discharges (available for 576 days) (Fig. 5a), which led to two linear relationships separated by the threshold NDWI value of 0.3. These relationships were subsequently used to predict Q_{daily} values in the 1993–2006 period, during which we do not have any daily discharge values.

Using both predicted and measured Q_{daily} values, we also calculated the number of days (NoD) when $Q > Q_1$. In braided rivers, bedload transport usually occurs with discharges much lower than Q_1, so that the number of days with $Q > Q_1$ reflects the duration of a year the formative discharge (i.e., Q_1) lasted (Bertoldi et al., 2010). If this is the case in our studied reach, then the NoD should be correlated with magnitudes of changes in channel morphology.

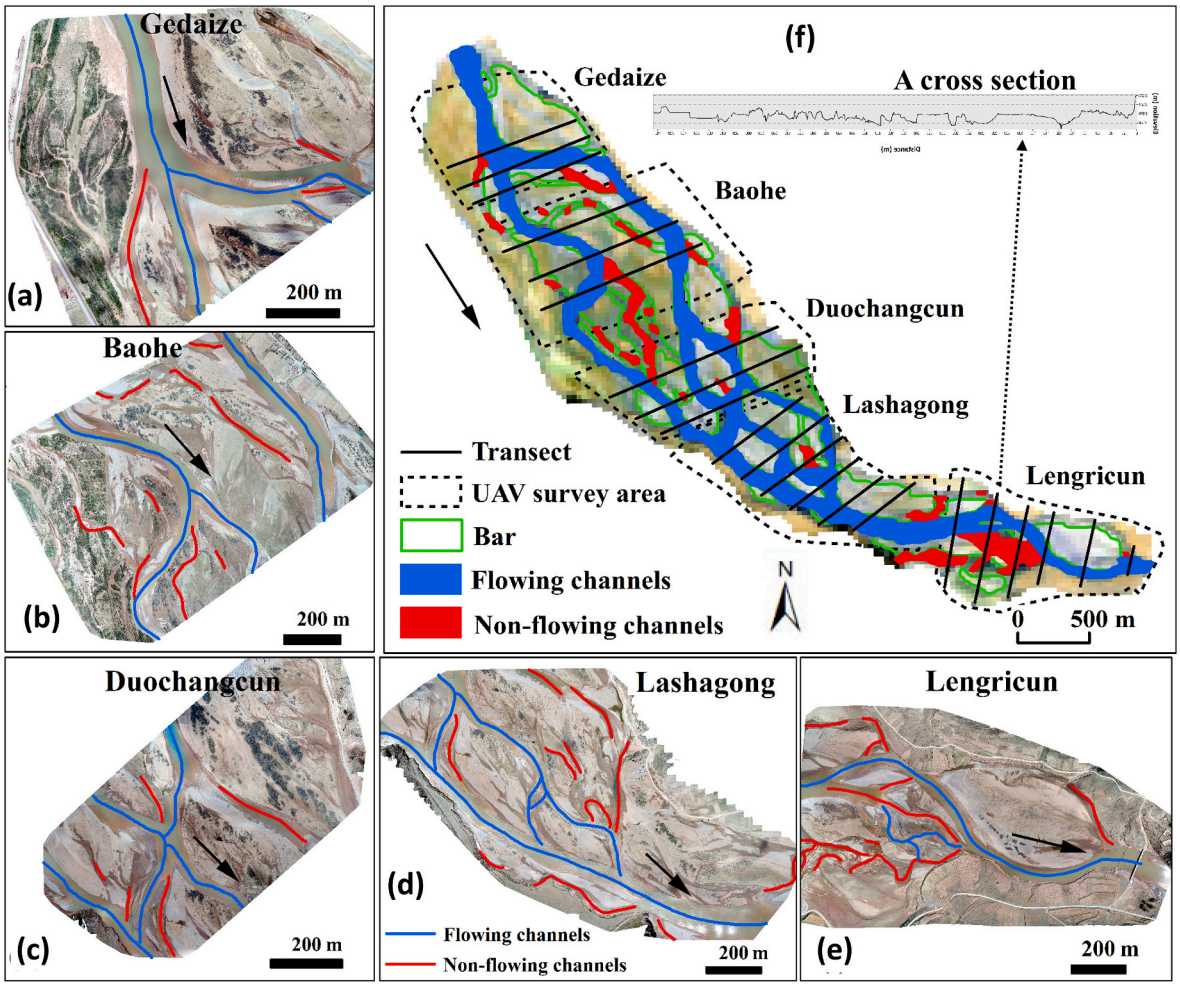

Fig. 4. Design of morphological calculations for channels and bars. (a)–(e) High-resolution ortho-images showing the two types of channels within the five surveyed sub-zones from upstream to downstream; and (f) The same two types of channels identified in the Landsat image of the same year. Also shown are transects selected for calculating channel morphology, distribution of the five surveyed sub-zones, and an example profile of a channel cross section along one of the selected transects.

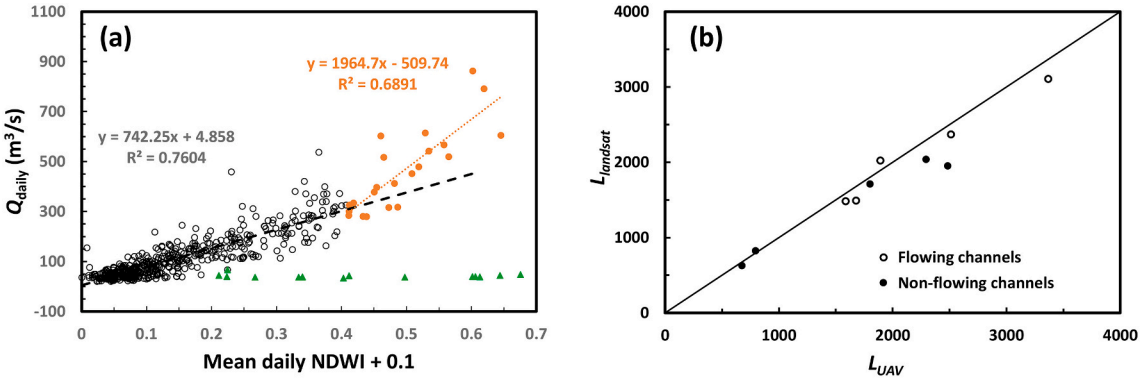

Fig. 5. (a) Empirical relationships between the mean daily NDWI and measured daily discharges (Q_{daily}); The green triangles are 'abnormal points', representing images covered by snow or ice that significantly affect the mean daily NDWI values; (b) Comparison of measured lengths of flowing and non-flowing channels using lengths derived from the UAV and Landsat images obtained in 2018.

2.3.2. Flowing and non-flowing channels

In each selected Landsat image, two types of water channels were identified and measured separately. The first are the main and secondary channels that are occupied by continuous (or connected) water bodies, forming flows from upstream to downstream. They are termed as flowing channels (Fig. 4f). The second are relatively smaller channels that are only connected to a flowing channel either at the upstream or downstream end, or that have disconnected water bodies. They are denoted as non-flowing channels (Fig. 4f). Both types of channels were identified using the Modified Normalized Difference Water Index (MNDWI), which is based on near infrared and short-wavelength infrared bands and has been proven more sensitive to water bodies (Xu, 2006; Zhou et al., 2015). The threshold value of MNDWI was determined by comparing lengths of two types of channels (i.e., their centerlines) identified from the five high-resolution UAV images obtained in 2018 (Fig. 4a–e) to those from the 2018 Landsat image (Fig. 4f). Our results showed that these lengths from two different types of images were comparable (Fig. 5b). Thus, these channel (centerline) lengths in other Landsat images were determined using the same index with similar threshold values.

2.3.3. Morphological metrics

Three morphological metrics were extracted from the selected images. The first is the active channel width (W_c, m), which refers to the total width of all channels and gravel bars without vegetation among channels. Gravel/sand bars are defined as the areas separated by water bodies and on the valley edges (Fig. 4f). Vegetation developed in the studied braided reach was distributed on these gravel bars. Therefore, W_c was calculated as the ratio of the total area of all channels and gravel bars excluding the vegetation area to the length of the alluvial valley. The first two types of areas were determined directly from the selected Landsat images, while the last one was calculated using Eq. (2) described in Section 2.3.4. The definition of W_c is consistent with that used in many earlier studies (Lallias-Tacon et al., 2017; Peixoto et al., 2009; Rozo et al., 2014; Werbylo et al., 2017).

The second metric is the annual lateral shifting rate of the main channel (R_s, m/yr). For each available peak Q (Q_{peak}), we identified a pair of images in the dry season before and after the peak flow and determined R_s, which is defined as the lateral change of the main flowing channel with the largest mean width. It was calculated as the ratio of the area bounded by the two centerlines of the main channels to the length of the centerline in the earlier year divided by the number of years between the two. We ignored the areas of changes that are less than 900 m^2 as they are more likely errors than real changes. The R_s was determined for the 12 Q_{peak} values, as there were no paired images available in three years. Although lateral migration in single-thread meandering rivers may be caused by bank erosion and cutoffs in braided rivers, lateral shifting of channels is driven by three different processes, (1) bank erosion, (2) avulsion (Ashmore, 2013; Bertoldi et al., 2010; Dunne and Jerolmack, 2018; Williams et al., 2015), or (3) choking of the channel (i.e., local avulsion) caused by the asymmetric configuration at the bifurcation nodes (Bertoldi and Tubino, 2005; Tubino and Bertoldi, 2008; Williams et al., 2015; Zolezzi et al., 2006).

The third metric is the mean braiding intensity (BI_t) for the flowing and non-flowing channels. The braiding intensity (BI_t) was defined as (Egozi and Ashmore, 2008)

$$BI_t = \sum_{i=1}^{N_{XS}} N_{Li} \Big/ N_{XS} \quad (1)$$

where N_{Li} is the number of flowing and the total (flowing and non-flowing) channels along the ith transect and N_{XS} is the total number of transects, which is 36 in this study (Fig. 4f). In this study, the first is referred to as the flowing BI_f, while the second is the total BI_t. The latter is equivalent to the 'total sinuosity index' (Hong and Davies, 1979) and 'the total braiding intensity' (Ashmore, 2013; Belletti et al., 2013) used in the previous studies. Following this notation, braiding intensity for non-flowing channels is denoted as BI_{nf}.

2.3.4. Changes in vegetated bar areas

Vegetated areas in Landsat images are commonly determined by calculating Normalized Difference Vegetation Index (NDVI) values (Ju and Masek, 2016; Ozyavuz et al., 2015; Rouse et al., 1973; Tucker, 1979). Although many studies have shown that NDVI = 0.2 is an appropriate threshold for identifying riparian vegetation (Bertoldi et al., 2013; Henshaw et al., 2013; Nagler et al., 2005), others indicated that this threshold value can vary depending on vegetation community types, such that different NDVI thresholds may exist for different land cover types or where there exists continuous correlation between percent vegetation coverage and NDVI values (Gallo et al., 2005; Marchetti et al., 2016; Powell et al., 2014; Purevdorj et al., 1998). Because the winter season was selected to obtain low flow conditions, in the studied braided reach, the vegetation density is relatively low, so that vegetation only occupies 50% or less of many pixels in an image, vegetation only occupies 50% of it or less. Thus, use of a single NDVI value for one pixel cannot predict vegetation area accurately.

This challenge may be resolved by obtaining high-resolution images using emerging new UAV technology in a field survey. While UAVs equipped with multispectral sensors may receive both visible light and infrared wavelengths for calculating indices such as NDVI to better identify vegetation types (Assmann et al., 2019), lightweight UAVs with a regular camera are more affordable and easier to operate. Nonetheless, the high-resolution images obtained using the DJI UAV used in this study only collected RGB (Red, Green, and Blue) bands. Although many

indices have been developed based on these three visible bands, such as Visible Atmospherically Resistant Index (VARI), Color Index of Vegetation Extraction (CIVE), Normalized green-red difference index (NGRDI) (Eng et al., 2018; Gitelson et al., 2002; Hague et al., 2006; Torres-Sánchez et al., 2014), these indices are site specific and lack generality. A more serious limitation of UAV images lies in the fact that no historical UAV data are available for extracting vegetation areas from a historical series of Landsat images. As such, we proposed an effective method of coupling both Landsat and regular UAV data to determine historical vegetation areas on gravel bars. Our approach was to develop an empirical relationship between vegetation areas identified from the UAV images acquired in 2018 and NDVI values calculated using the Landsat image of the same month of the year, and then to extend the relationship to other years for calculating the associated vegetation areas. Detailed steps of the method are described as follow.

The first step was to develop an empirical index that may efficiently identify trees and shrubs on gravel bars in the UAV ortho-photo. Adopting the formula for the NDVI, we experimented with different combinations of RGB bands and the fourth (reference) band in UAV images and found that the index based on the red and reference bands may be most efficiently used to identify trees and shrubs. In the second step, individual areas of trees and shrubs were first automatically identified by calculating this index in ENVI 5.0 and were subsequently examined manually and corrected wherever errors were found. The operation accurately extracted boundaries of separated vegetation clusters in the studied reach (Fig. 6a). Next, the vegetation area detected on UAV images (A_v%) was calculated in each Landsat pixel (30 × 30 m) as a percentage. The third step produced a plot of A_v% versus NDVI values for all Landsat pixels included in the UAV ortho-photo, which showed that for pixels with NDVI < 0.1, A_v% was less than 10 for almost all pixels. Visual check of these pixels in the UAV ortho-photo indicated that vegetation coverage was very small and may be ignored. In the fourth step, we investigated the nature of the scattered data for pixels with NDVI > 0.1 by grouping them into several classes that had similar NDVI values but different A_v%, and similar A_v% but different NDVI values. This showed that most pixels with an 'abnormally' large A_v% indeed included a significant proportion of grass. Given that the potential impact of vegetation on gravel bars in a braided river is mostly caused by trees and shrubs, pixels with a significant amount of grass areas were eliminated. In the last step, values of NDVI and A_v% were used to develop an empirical A_v%-NDVI relationship (Fig. 6b). Values of A_v% in pixels with NDVI around 0.26 and 0.33 were relatively high, indicating relatively higher degrees of uncertainties in predicting A_v% values for pixels with NDVI falling around these two classes. However, the means of A_v% values were well correlated with the middle values of the pixel NDVI in all classes:

$$A_v\% = 2.632e^{8.767NDVI} \quad R^2 = 0.89, p < 0.05 \tag{2}$$

To validate Eq. (2), we estimated A_v% by three different methods and compared them. In the first method, we selected the only available Google Earth image (with the resolution of 0.6 m) for the studied reach in 2014 and determined A_v% by identifying vegetation areas from this image and summing all of them (Fig. 6c). In the second method, we calculated NDVI values for the 2014 Landsat image and used Eq. (2) to determine A_v%. In the third method, we identified vegetation areas in the 2014 Landsat image by setting up a threshold value of NDVI and calculated A_v%. The results showed that A_v% was 0.22, 0.29, and 0.94 for the three methods, respectively. The third method of directly counting cells with NDVI above the threshold significantly overestimated A_v% (Fig. 6c). Therefore, Eq. (2) was sufficiently accurate for determining A_v% in other years with selected Landsat images.

3. Results

3.1. Effects of morphodynamics on braided planform

Visual analysis of the annual mean flow pattern from Google Earth Engine (GEE) Landsat resources showed that the braided pattern of the river mainly evolved during specific years: 1989, 1994, 2000–2001, and 2014(see Supplementary Fig. S2). Although some bends have moved, the main channel has not changed drastically. The flow pattern has apparently stayed relatively stable over periods with generally low braiding intensity for the 1986–1988, 1994–1999, and 2009–2013 periods, whereas in other periods (i.e., 1989–1994; 2000–2008; 2017–2018), braided activity with multiple and more active flow channels were observed, but then decreased progressively in the following years.

To test how these inter-annual geomorphic changes affect braided channel network, we first studied the interannual variability of the flowing braiding intensity (Fig. 7a). We found that there is a strong correlation (R^2 = 0.66) between the braiding intensity of flowing channels (BI_f) and the Q_{daily} value on the same day when the image was obtained, although seasonal variations can be clearly observed (Fig. 7a). This positive relationship indicates that increasing discharges can lead to more flowing channels in the studied braided reach. Thus, although the images were all obtained in the dry season when Q_{daily} values were low with less variability, we still adjusted the BI_f values by scaling them using $Q_{daily}^{0.25}$, which is based on the BI_f - Q_{daily} relationship, to eliminate changes in braiding intensity purely caused by discharge variations (Fig. 7a). From 1989 to 2018, BI_f generally decreased, but showed different temporal trends in four stages (Fig. 7b). In the early period between 1989 and 2000, the corrected BI_f decreased almost linearly

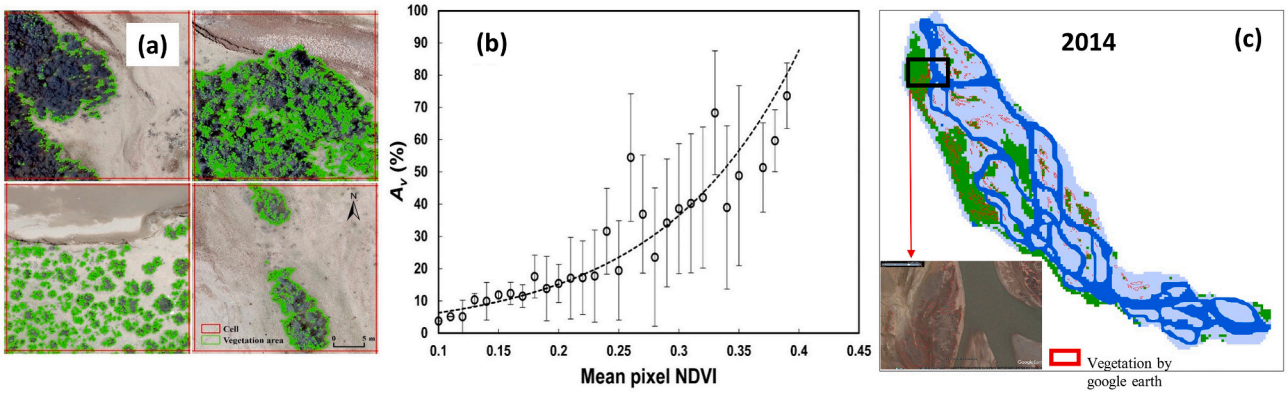

Fig. 6. A method of determining vegetation areas on gravel bars in the studied braided reach. (a) Illustration of the calculation of vegetation areas within four Landsat pixels that have different percentages of vegetation; (b) The established relationship between NDVI values and the associated percentages of vegetation within each pixel of the Landsat image (Eq. (2)); (c) Validation of Eq. (2) using the Google Earth image in 2014. The green color represents the vegetation areas calculated using NDVI values and the red boundaries distinguish the vegetation areas within the Google Earth image.

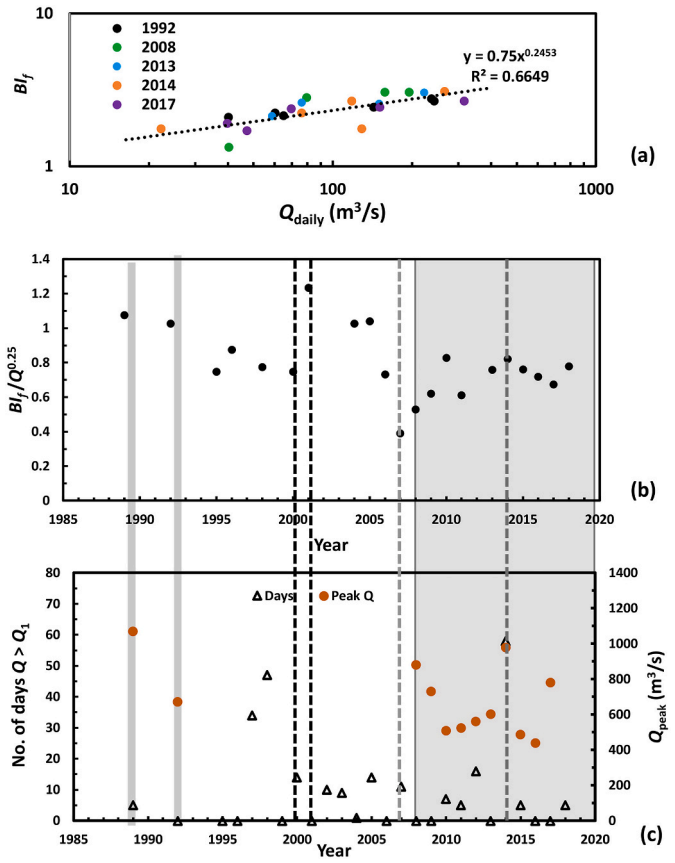

Fig. 7. Morphodynamic characteristics of the flowing channels. (a) the relationship between BI_f (flowing braiding intensity) and the associated daily Q; (b) Temporal changes of the adjusted BI_f; (c) Temporal changes of the hydrological magnitude and frequency. The gray sections represent the years when daily discharges are available. The dashed vertical lines mark different temporal trends of braiding intensity.

except for a lower value in 1995. In the second stage between 2001 and 2009, it decreased with a much higher rate, while in the third stage (2009–2014), it began to increase most of the time. The corrected BI_f values in the latest stage between 2014 and 2018 varied within a limited range, decreasing slightly. These trends are coherent with the previously described visual observation, indicating that braided activity has evolved through time and this evolution reflected geomorphic response of the studied reach to high flows. A resetting of the braided activity occurred abruptly in 2001 or over several years as observed between 2009 and 2014.

Using the available time series of discharges (gray sections in Fig. 7b and 7c), we observed that the decrease of braiding intensity in the 1989–1990 and 2014–2015 periods corresponded well with the associated decreases of annual peak discharges (Q_{peak}) (Fig. 7c). However, from 2007 to 2008, the decrease of Q_{peak} corresponded to an increase of braiding intensity. These complex patterns suggest that braiding intensity is linked to peak discharges through different fluvial events that led to different behaviors of river morphology. Specifically, a reactivation of the braided activity might be caused by ample sediment input in the reach that promoted some avulsion processes, activating some secondary branches (e.g., in the 1989–1990 and 2014–2015 periods), while a deactivation of the braided activity occurred in the 2007–2008 period when less sediment input facilitated bed incision of the main branches. Small readjustments were often observed in several years after these large events (i.e., larger changes of Q_{peak}). Because no measured Q_{daily} values are available in 2000 and 2001, and the available Q_{peak} values are not well correlated with the associated NoD, we have no evidence to show why BI_f increased significantly from 2000 to 2001. Nonetheless, it is possible that a large Q_{peak} in 2000 caused this increase. If this assumption is correct, then high discharges, rather than NoD could be one of the driving forces controlling temporal changes of channel structure.

Similarly, values of R_s showed no simple correlation with Q_{peak} values from 1989 to 2017 (Fig. 8a). The higher Q_{peak} values in 1989 and 2009 were associated with relatively larger R_s values, but the largest R_s value occurred in 2010 when the Q_{peak} was much lower. Also, Q_{peak} values were higher in 2008 and 2017 than in 2009, but were associated with very low R_s values. The paired 2008–2009 images (Fig. 8b) showed that relatively low R_s values were caused by asymmetric bifurcation, which means that the main channel shifted to its existing neighboring channel. Thus, the relatively high Q_{peak} in 2008 (880 m^3/s) created a few small flowing channels, which accounted for the increase of BI_f from 2008 to 2009 (Fig. 7b). However, the paired 2009–2010 images showed that a relatively high R_s was caused by avulsion, which scoured the braidplain and connected to an old channel (Fig. 8c). Therefore, though the Q_{peak} in 2009 (732 m^3/s) was less than that in 2008, it tended to create more flowing channels, leading to greater increase of BI_f from 2009 to 2010, compared to that from 2008 to 2009 (Fig. 7b). From 2010 to 2011, the lateral change of the main channel was caused by extensive bank erosion, which happened in multiple segments along the entire studied reach (Fig. 8d), leading to the highest R_s value over the entire study period (Fig. 8a). It is interesting to note that the associated Q_{peak} value (510 m^3/s) was much lower than the previous two. Apparently, this peak flow was insufficient to alter the course of the main channel by either asymmetric bifurcation or avulsion. It seems that higher R_s values did not occur with peak flows but needed progressive channel changes (aggradation) as a preparation phase before avulsion occurred and the braiding pattern was reset. This can be further evidenced in 2016 to 2017 when the R_s value was relatively low, but Q_{peak} was much higher (780 m^3/s) (Fig. 8e).

3.2. Seasonal changes of non-flowing channels and hydrological implications

We also observed from GEE Landsat resources a potential seasonal pattern in non-flowing channels. By separating mean daily NDWI values in spring from those in fall and comparing them against the daily discharges over the same period of years, we showed that for the same Q_{daily} value, spring and fall tended to have similar mean daily NDWI values (Fig. 9a), though fall might have higher NDWI values for relatively higher Q_{daily} values. This similarity suggests that water channels tended to have similar wetted areas in spring to those in fall.

Non-flowing braiding intensity (BI_{nf}) was on average similar in spring (April and May) to that in fall (October and November) during 1992, though the associated daily discharges (Q_{daily}) were actually lower in spring than those in fall (Fig. 9b). A similar trend was found in 2017 (Fig. 9c). Extending to all years with measured daily discharges and seasonal images, BI_{nf} (expressed as the ratio of BI_{nf} to BI_t for the purpose of eliminating the potential effect of discharge variations among the obtained images) on average is marginally higher in spring than in fall and the average Q_{daily} is again lower in spring than in fall (Fig. 9d). However, the difference of BI_{nf} between spring and fall is not statistically significant. A possible explanation is that this difference is embodied not only in the number of channels, but also their lengths.

Calculating braiding intensity for both flowing and total channels in the five segments along the studied braided reach (Fig. 4f) signified that the braided structure, highlighted by the ratio of non-flowing to flowing channels remains similar along the entire studied reach (Fig. 10), even though the valley becomes narrow in the downstream segment owing to bedrock constraint (Fig. 4f). Therefore, the previously described tendency of more groundwater flows supplied to non-flowing channels in spring than in fall (Fig. 9) remains true across the entire studied reach.

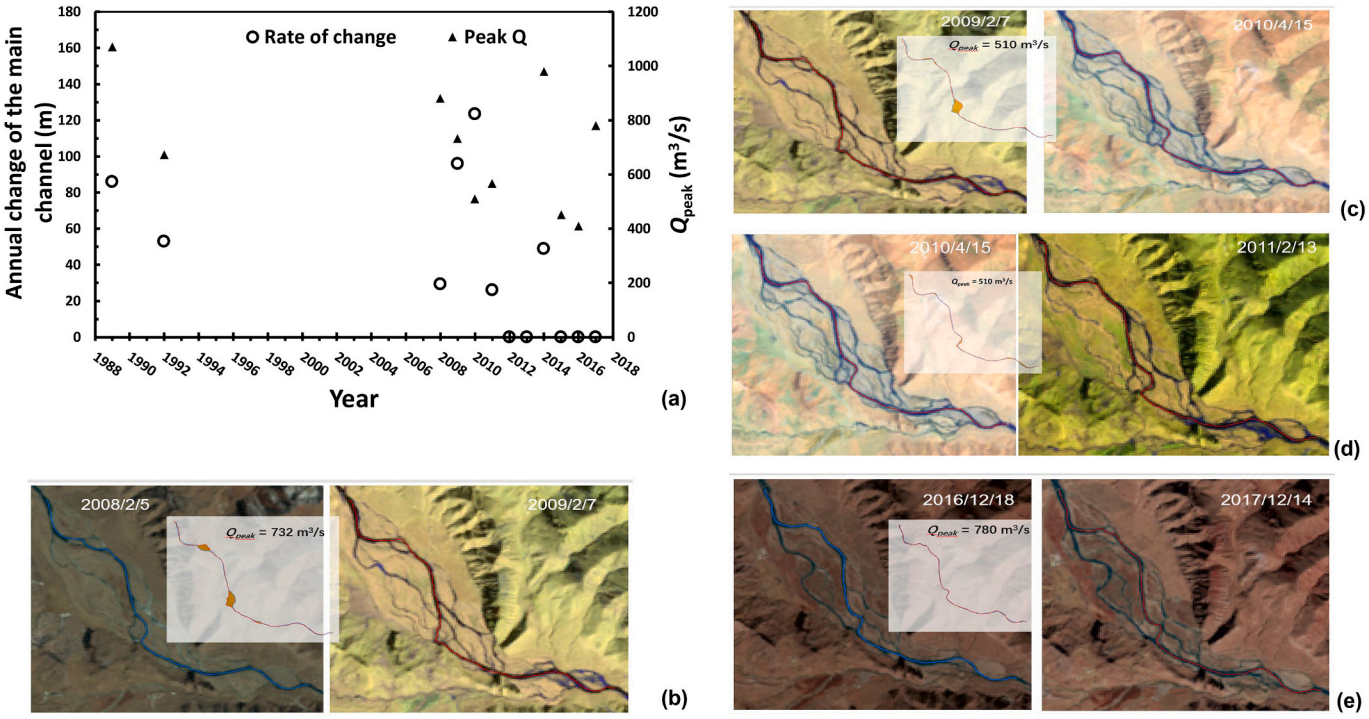

Fig. 8. (a) Main channel changes in the years with measured peak discharges. (b)–(e) Four image pairs showing locations of the changes in these four years.

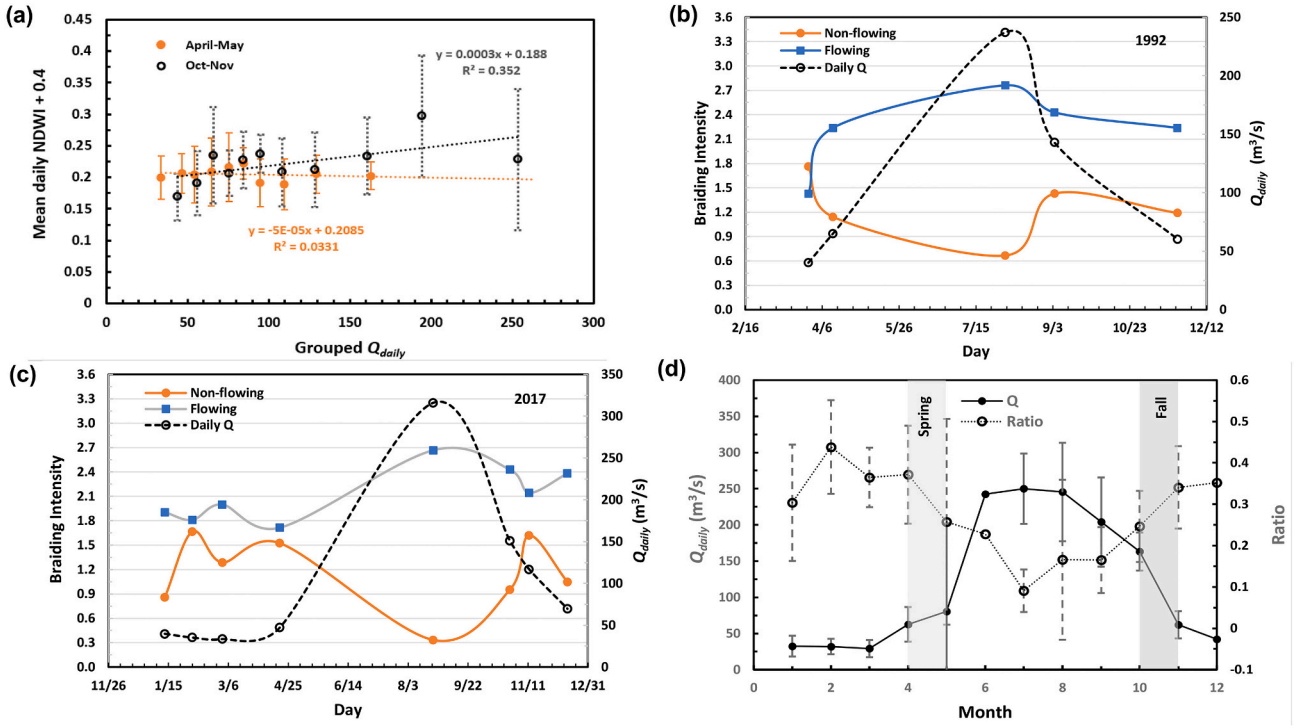

Fig. 9. Seasonal changes of non-flowing channels in the years with measured daily discharges. (a) The relationship between water areas and daily Q for spring and fall; (b) and (c) Seasonal variations of braiding intensity in 1992 and 2017; (d) Monthly mean Q_{peak} and the ratio of BI_{nf} to BI_t.

3.3. Temporal changes of vegetation on gravel bars

Vegetation area on bars (A_v) increased briefly from 1989 to 1992, and then decreased during the period between 2005 and 2009 (Fig. 11a). It subsequently increased faster and reached the maximum at the end of the last period (2009–2018). The percentage of A_v in the total bar area varied from 5% to 22% with the mean of 11%, indicating that vegetation cover in the studied braided reach was generally low. Temporal changes of the active channel width mirroring those of vegetation generally decreased over time (Fig. 11a), showing that vegetation encroachment has gradually reduced the braidplain area available for channel creation and shifting after 2000. No clear link was established

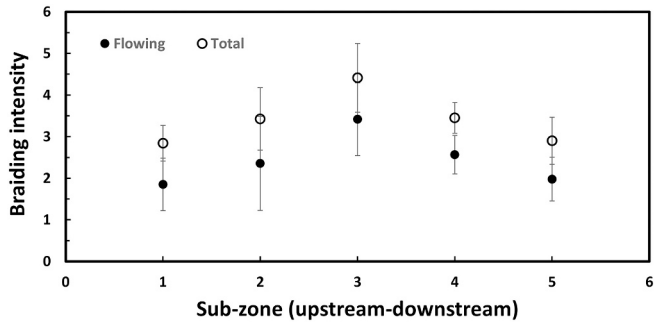

Fig. 10. Spatial patterns of braiding intensity for flowing and total channels.

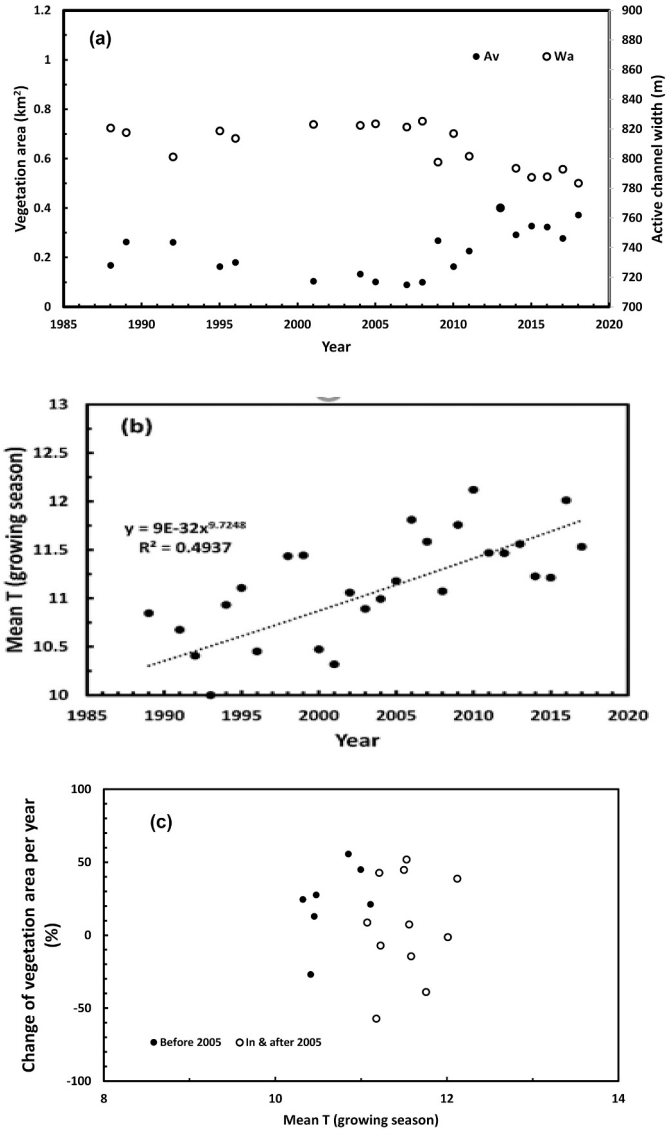

Fig. 11. Temporal characteristics of vegetation, active channel width, and temperature. (a) Temporal changes of vegetation area and active channel width; (b) Temporal trend of mean temperature in the growing season (MTGS); (c) Annual change of vegetation areas vs MTGS.

with peak flows and their changes in braided regime because the temporal trend of available Q_{peak} (Fig. 7c) is not correlated to that A_v (Fig. 11a). The braided pattern reactivation in the 1989–1990 or 2000–2001 periods did not have any effects on vegetation cover, which was reflected by the almost unchanged Av in the same period (Fig. 11a). Vegetation encroachment (i.e., increase of A_v) was quite abrupt from 2008 to 2013, which was a period when braided activity increased progressively (Fig. 7b). It stopped after 2014 when braided activity was slightly high (Fig. 7b).

Over the entire study period from 1989 to 2018, the mean temperature of the growing season (i.e., from the middle of June to the end of September) (T_g) generally increased with time, although the scattered variation of T_g was discernable (Fig. 11b). It appears that a shift occurred in 2005, after which the interannual variability of T_g (i.e., coefficient variation (CV) = 0.030) remained the same as before (i.e., CV = 0.028), but the mean interannual temperature was significantly higher. The annual percent change (APC) of A_v in the periods before and after 2005 were not discernably correlated to the associated T_g (Fig. 11c). However, the average APC of A_v in the two periods was 10.72 and 12.94, respectively. The associated mean T_g was 11.56 and 13.20, respectively. It indicated that on average A_v experienced a lower degree of annual change with lower T_g in the earlier period (i.e., 1989–2005) than in the later period (i.e., 2006–2017). These patterns suggest that (1) the mean of T_g during the study period of five decades tends to influence vegetation development on gravel bars, and (2) the degree of T_g variation also affects changes of A_v.

4. Discussion

4.1. Do braided planform and morphodynamics reflect low resistance or high sediment supply?

In the relationship between the active channel width (W_c) and watershed area (Fig. 12a), our studied reach was plotted above those in European alpine river systems based on the data from (Piégay et al., 2009), suggesting that the ULR reach is likely to be a well-connected river system with sufficient sediment supply. This morphologic characteristic is further supported using the normalized bed relief index (*BRI**), defined as the ratio of the standard deviation of elevations in an active channel to the channel width (see Fig. 3 in Liebault et al., 2013). The mean *BRI** value calculated over 15 cross sections of the studied reach using our UAV data (Fig. 3f) was 0.0013, which is lower than those of the 31 alpine reaches measured by Liebault et al. (2013). It is also well known that vegetation actively imposes an additional resistance to flow and hence helps stabilize morphological structures of channels and bars (Bertoldi et al., 2011; Tal et al., 2004). This effect has been widely incorporated into physically based models for predicting the complex interaction between fluvial processes and morphological responses of braided rivers (Camporeale et al., 2013; Limaye, 2017; Redolfi et al., 2016).

Thus, the larger W_c of the ULR reach relative to those of the braided rivers draining through more vegetated corridors in European alpine systems can also be partly attributed to the fact that the sparse vegetation in the ULR reach reduces bank resistance and facilitates bedload movement. This also suggests that wide active channels and wider sections of braided corridors with typically low BRI* may be potentially hot spots of interactions between groundwater and surficial water. It follows that the active channel width should be explored more extensively at the regional scale of the Qinghai-Tibet Plateau by considering reaches above and below the elevation limit of tree development to better separate the effect of bedload supply from that of local resistance caused by vegetation encroachment on the active channel width.

Our result that larger R_s may not necessarily be caused by high flows (Fig. 8a) suggests that shifting of the main channel from the development of an asymmetrical channel configuration (Bertoldi and Tubino, 2005; Tubino and Bertoldi, 2008) was most efficiently caused by moderately high competent flows, which was consistent with earlier studies in the Alps and other braided reaches (Bertoldi et al., 2010; Li et al., 2008). This result also supports our finding that the temporal pattern of the braided activity is not fully attributed to the two well-

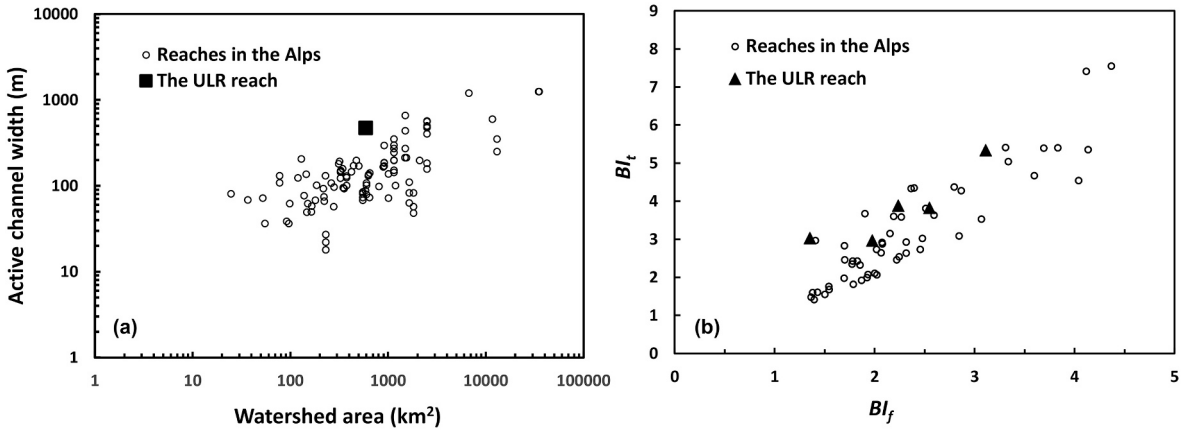

Fig. 12. Comparison between the ULR reach and those in European Alps. (a) Active channel width (m) vs watershed area (km^2); and (b) Total braiding intensity (BI_t) vs flowing braiding intensity (BI_f).

known factors, peak flows and vegetation resistance.

We observed that although peak flows could partly explain braided network resetting, they are not the cause of shifting and avulsion. This fact indicates that river morphodynamics is linked to not only flow magnitudes, but also the nature of the braided structure in term of sediment transfer. Moreover, different magnitudes of flows may lead to different geomorphic responses. We may also expect, as observed in flume, discontinuous bedload movement at the instantaneous temporal scale (Peirce et al., 2018), or those at the event scale (Liebault et al., 2012; Liebault and Laronne, 2008; Misset et al., 2020). This discontinuous bedload-transport mode suggests that in the studied ULR reach the spatial irregularity of short-term sediment pulses on channel morphology may have quite random effects on channel avulsion that are potentially a mismatch with magnitudes of peak flows.

Regarding vegetation resistance in the ULR reach, the fact that the moderately high Q_{peak} in 2009 (732 m^3/s) created relatively more channels (Fig. 8a) by avulsion (Fig. 8b) may be attributed to the lack of vegetation because vegetation cover in the braidplain was lower in this year (Fig. 11a). On the contrary, a slightly higher Q_{peak} in 2017 (780 m^3/s) only caused limited bank erosion (Fig. 8e) with no new channel created (Fig. 7b) because the vegetation area in 2017 was much higher than that in 2009. It also should be noted that there is no clear signal showing that upstream human activities have had any significant impact on the morphodynamics of the studied reach.

4.2. Interaction between groundwater and surface flows

Fig. 12b shows that the total (both flowing and non-flowing) BI_t of the ULR is generally higher than those of Alpine braided reaches (Belletti et al., 2013) showed that the ULR reach is situated on the upper set of reaches studied in the Alps (Fig. 12b), signifying that the channel structure of the ULR reach is very well characterized by upwelling areas and non-flowing channels. Therefore, non-flowing channels and their surrounding braidplains should be potentially good habitats for the aquatic fauna that are supported by upwelling processes if functioning is comparable to that observed in low elevation systems (Bertoldi et al., 2011; Malard et al., 2006).

It is surprising to observe that groundwater supply to non-flowing channels was similar in spring and fall (Fig. 9a and d). The groundwater is expected to be recharged by floods or relatively high flows and logically should be highest after the flood season. Therefore, our observation suggests that this higher-than-expected intensity of non-flowing channels during spring may be linked to other factors, such as the impermeability of alluvium. If the alluvium is frozen, water in surface cannot be absorbed so that this functioning may be a characteristic of such high-altitude systems.

In the Val Roseg reach of the Swiss Alps, longitudinal variation of flowing and total BI_t is characterized by an upstream zone of downwelling and a downstream zone of upwelling caused by a significant increase of downstream non-flowing channels at the very end of a large valley downstream of a bottleneck (Malard et al., 2006). In contrast, the ULR reach demonstrates an even spatial distribution of flowing and total BI_t (Fig. 10), even though valley morphology changes in the longitudinal direction (Fig. 4f). This spatial pattern and the unexpected higher frequency of non-flowing channels in winter underscore the need for more field research to better understand the aquifer characteristics and its link to the surficial water to provide additional information for better interpreting remote observations.

4.3. Causes of vegetation changes

Our results on vegetation patterns (Fig. 11a) give rise to two intriguing questions: (1) Why was the vegetation cover reduced by 50% between 1989 and 2008? (2) What might be responsible for the relatively abrupt encroachment between 2009 and 2014? We believe that the reduced vegetation cover might be linked to the combination of scouring process and vegetation mortality. The braided reactivation in 1989 did not seem to fully explain the scouring mechanism as vegetation cover increased from 20% to almost 30% in 1989 and was still high in 1992. However, the 2000 reactivation event may explain decrease in vegetation from 20% to 10%. Therefore, vegetation mortality related to changes in habitat conditions may play a role in the temporal reduction of vegetation cover, but should be further explored using field monitoring. For the second question, we argue that the mean temperature of the growing season (T_g) may be one of the main factors controlling changes of vegetation growth and extent (Fig. 11c), as it has been shown in the Alps by Raepple et al. (2017). However, in our case, changes of temperature and vegetation cover were not well correlated with each other (Fig. 11c), suggesting the possible roles of other factors. The relatively high peak flows in 2008–2009 and the low peak flows from 2010 to 2014 seem to suggest that young plants were not really scoured during this temporal sequence (Fig. 7b). This might promote recruitment, resulting in the increase of vegetation areas in this period (Fig. 11a), which may be supported by the well-known recruitment box model (Mahoney and Rood, 1998). In addition, the state of braided planform structure and the associated temperature in 2009 might provide an optimal ecological setting that promoted plant growth and recruitment.

Unfortunately, it is impossible to disentangle these factors without more detailed information that needs to be obtained from more field work. Alternatively, it might be more important to ask whether this braided system will stay encroached or experience scouring in the

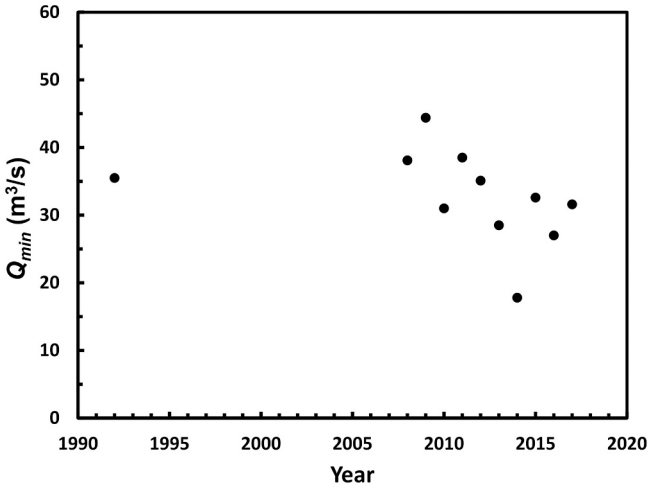

Fig. 13. Daily discharges in the days when Landsat images were available.

future. We are certain that low flows had been decreasing since 2009 (Fig. 13). Because the low flow period occurred during the vegetative dormancy period, it does not influence vegetation growth and recruitment and hence gives way to temperature as the dominant factor of controlling vegetation changes. This functioning is obviously different from what has been observed in braided Mediterranean channels where the vegetation growth and the low flow season is in phase. If low flow will maintain the current trend, then we expect weakened upwelling processes and diverse aquatic habitat that can adversely affect biodiversity of the ULR system.

5. Conclusions

Little is known about braided rivers in high-elevation regions, though they often play important roles in the associated cold and fragile riverine ecosystem. A typical braided river reach within the Upper Lancang River (ULR), located on the Qinghai-Tibet Plateau with elevations ranging between 3400 and 3700 m, was examined remotely using a high-resolution time series of Landsat images and a high spatial-resolution ortho-image obtained using an Unmanned Aerial Vehicle (UAV) in May 2018. Analyzing temporal changes and the interaction of metrics that may sufficiently characterize morphological properties of braided channels and the dividing gravel bars in the studied braided reach enabled us to make the following conclusions:

(1) The studied ULR reach seems to be a braided river system that is abundantly supplied with sediment compared to reaches in the European alpine river system and others. We showed that the main channel has shifted over time and the braiding activity has evolved through time according to peak flows. This potentially well-connected braided system with sufficient sediment supply may be caused by less vegetation cover and lower surface roughness, such that potential sediment waves are able to pass through it, temporally increasing active channel width and associated total braiding intensity with channel shifting and local avulsions. The stability of the main channel over several years and successive floods was unexpected and these processes contrast to those observed in the braided reaches of the European Alps, such that a significant thermal mosaic exists within the braided environment with potential room for ecological refugees.

(2) Braiding intensity is sensitive to variable low flows. About 30% of the braided channels are disconnected even during low flows. The degree of connectivity between surficial and groundwater in the ULR reach is much higher than many reaches in the European Alps.

(3) Temporal variation of vegetation areas on gravel bars in the ULR braided reach seems to be controlled by not only channel morphodynamics and scouring, but also optimal recruitment windows as shown elsewhere. Additional field work is needed for better understanding vegetation mortality, scouring, recruitment and growth to reveal the underlining mechanisms.

(4) Our method of combining UAV data with the concurrent Landsat image to assess the flowing/non-flowing channel network and vegetation areas in historical Landsat images within the braided zone was proven to be a reliable means of obtaining data. The increased use of UAV technology to obtain high-resolution images will make this method more valuable in the future for studying groundwater-surficial water interactions and riparian vegetation in braided rivers, and to determine if the ULR reach is unique in the Qinghai-Tibet Plateau or representative of most braided rivers in term of functioning and temporal trajectories. Furthermore, we showed the first time the great advantage of using NDWI values obtained via GEE to assess daily discharges that cannot be measured directly and detect major channel shifts.

Declaration of competing interest

The authors declare that they have no known competing financial interests or personal relationships that could have appeared to influence the work reported in this paper.

Acknowledgements

This study was supported by the National Natural Science Foundation of China (51979012), Fundamental Research Funds for the Central Universities (2042021kf0199), Natural Science Foundation of Hunan Province (2020JJ3036), Natural Science Foundation of Hubei Province of China (2020CFB554), and Central Public-interest Scientific Institution Basic Research Fund (CKSF2021743). This work was also performed within the framework of the EUR H2O'Lyon (ANR-17-EURE-0018) of Université de Lyon, within the program 'Investissements d'Avenir' operated by the ANR. We thank Hanyuan Yang, Dongfeng Li, Hanyou Lu, and Xu Yan for their assistance in field survey and data processing.

Appendix A. Supplementary data

Supplementary data to this article can be found online at https://doi.org/10.1016/j.geomorph.2022.108180.

References

Ashmore, P., 2013. Morphology and dynamics of braided rivers. In: Shroder, J., Wohl, E. (Eds.), Treatise on Geomorphology. Academic Press, San Diego, CA, pp. 289–312.
Assmann, J.J., Kerby, J.T., Cunliffe, A.M., Myers-Smith, I.H., 2019. Vegetation monitoring using multispectral sensors – best practices and lessons learned from high latitudes. J. Unmanned Vehicle Syst. 7, 54–75.
Belletti, B., Dufour, S., Piegay, H., 2013. Regional variability of aquatic pattern in braided reaches (example of the French Rhone basin). Hydrobiology 712, 25–41.
Belletti, B., Dufour, S., Piegay, H., 2015. What is the relative effect of space and time to explain the braided river width and island patterns at a regional scale? River ResApplica. 31, 1–15.
Bertoldi, W., Drake, N.A., Gurnell, A.M., 2011. Interactions between river flows and colonizing vegetation on a braided river: exploring spatial and temporal dynamics in riparian vegetation cover using satellite data. Earth Surf. Process. Landf. 36, 1474–1486.
Bertoldi, W., Tubino, M., 2005. Bed and bank evolution of bifurcating channels. Water Resour. Res. 41, W07001. https://doi.org/10.1029/2004WR003333.
Bertoldi, W., Zanoni, L., Tubino, M., 2009. Planform dynamics of braided streams. Earth Surf. Process. Landf. 34, 547–557.
Bertoldi, W., Zanoni, L., Tubino, M., 2010. Assessment of morphological changes induced by flow and flood pulses in a gravel bed braided river: the Tagliamento River (Italy). Geomorphology 114, 348–360.
Bertoldi, W., Zanoni, L., Tubino, M., 2013. Assessment of morphological changes induced by flow and flood pulses in a gravel bed braided river: the Tagliamento River (Italy). Geomorphology 114, 348–360.

Camporeale, C., Perruca, E., Ridolfi, L., Gurnell, A.M., 2013. Modeling the interactions between river morphodynamics and riparian vegetation. Rev. Geophys. 51, 379–414.
Carley, J.K., Cavalli, M., Vericat, D., Crema, S., Llena, M., Beinat, A., Marchi, L., Cazorzi, F., 2012. Significant decadal channel change 58–67 years post-dam accounting for uncertainty in topographic change detection between contour maps and point cloud models. Geomorphology 179, 71–88.
Cienciala, P., Pasternack, G.B., 2017. Floodplain inundation response to climate, valley form, and flow regulation on a gravel-bed river in a Mediterranean-climate region. Geomorphology 282, 1–17.
Cucchiaro, S., et al., 2019. Geomorphic effectiveness of check dams in a debris-flow catchment using multi-temporal topographic surveys. Catena 174, 73–83.
Dunne, K.B.J., Jerolmack, D.J., 2018. Evidence of, and a proposed explanation for, bimodal transport states in alluvial rivers. Earth Surf. Dyn. 6, 583–594.
Egozi, R., Ashmore, P., 2008. Defining and measuring braiding intensity. Earth Surf. Process. Landf. 33, 2121–2138.
Egozi, R., Ashmore, P., 2009. Experimental analysis of braided channel pattern response to increased discharge. J. Geophys. Res. 114, F02012. https://doi.org/10.1029/2008JF001099.
Elosegi, A., Diez, J., Mutz, M., 2010. Effect of hydromorphological integrity on biodiversity and functioning of river ecosystems. Hydrobiologia 657, 199–215.
Eng, L.S., Ismail, R., Hashim, W., M A Raj Mohamed, R., Baharum, A., 2018. Vegetation monitoring using UAV: A preliminary study. Int. J. Eng. Technol. 7, 223–227.
Gallo, K., Li, L., Reed, B., Eidenshink, J., Dwyer, J., 2005. Multi-platform comparisons of MODIS and AVHRR normalized difference vegetation index data. Remote Sens. Environ. 99, 221–231.
Gitelson, A.A., Kaufman, Y.J., Stark, R., Rundquist, D., 2002. Novel algorithms for remote estimation of vegetation fraction. Remote Sens. Environ. 80, 76–87.
Grumbine, R.E., Dore, J., Xu, J.C., 2012. Mekong hydropower: drivers of change and governance challenges. Front. Ecol. Environ. 10, 91–98.
Gurnell, A.M., 2014. Plants as river system engineers. Earth Surf. Process. Landf. 39, 4–25.
Gurnell, A.M., Bertoldi, W., Corenblit, D., 2012. Changing river channels: the roles of hydrological processes, plants and pioneer fluvial landforms in humid temperate, mixed load, gravel bed rivers. Earth Sci. Rev. 111, 129–141.
Hague, T., Tillett, N.D., Wheeler, H., 2006. Automated crop and weed monitoring in widely spaced cereals. Precis. Agric. 7, 21–32.
Henshaw, A.J., Gurnell, A.M., Bertoldi, W., Drake, N.A., 2013. An assessment of the degree to which Landsat TM data can support the assessment of fluvial dynamics, as revealed by changes in vegetation extent and channel position, along a large river. Geomorphology 202, 74–85.
Hong, L.B., Davies, T.R.H., 1979. A study of stream braiding. Geol. Soc. Am. Bull. 90, 1839–1859.
Horn, J.D., Joeckel, R.M., Fielding, C.R., 2012. Progressive abandonment and planform changes of the Central Platte River in Nebraska, Central USA, over historical timeframes. Geomorphology 139, 372–383.
Huber, E., Huggenberger, P., 2015. Morphological perspective on the sedimentary characteristics of a coarse, braided reach: Tagliamento River (NE Italy). Geomorphology 248, 111–124.
Hugue, F., Lapointe, M., Eaton, B.C., Lepoutre, A., 2016. Satellite-based remote sensing of running water habitats at large riverscape scales: tools to analyze habitat heterogeneity for river ecosystem management. Geomorphology 253, 353–369.
Jax, K., 2005. Function and "functioning" in ecology: what does it mean? Oikos 111, 641–648.
Javernick, L., Brasington, J., Caruso, B., 2014. Modeling the topography of shallow braided rivers using structure-from-motion photogrammetry. Geomorphology 213, 166–182.
Ju, J., Masek, J.G., 2016. The vegetation greenness trend in Canada and US Alaska from 1984–2012 Landsat data. Remote Sens. Environ. 176, 1–16.
Kasai, M., Aoki, D., Peacock, D., Marutani, T., 2019. Channel evolution controlled by valley configuration during 70 years in a severely erosive catchment: Mangaoporo River, New Zealand. Catena 174, 324–338.
Kummu, M., Lu, X.X., Wang, J.J., Varis, O., 2010. Basin-wide sediment trapping efficiency of emerging reservoirs along the Mekong. Geomorphology 119, 181–197.
Lallias-Tacon, S., Liebault, F., Piegay, H., 2017. Use of airborne LiDAR and historical aerial photos for characterising the history of braided river floodplain morphology and vegetation responses. Catena 149, 742–759.
Leduc, P., Ashmore, P., Gardner, J.T., 2015. Grain sorting in the morphological active layer of a braided river physical model. Earth Surf. Dyn. 3, 577–585.
Li, S.S., Millar, R.G., Islam, S., 2008. Modelling gravel transport and morphology for the Fraser River Gravel Reach, British Columbia. Geomorphology 95, 206–222.
Li, Z., Lu, H., Gao, P., You, Y., Hu, X., 2020. Characterizing braided river systems of two nested watersheds in the source region of Yangtze RiverChina. Geomorphology 351, 10694.
Liebault, F., Bellot, H., Chapuis, M., Klotz, S., Deschatres, M., 2012. Bedload tracing in a high-sediment-load mountain stream. Earth Surf. Process. Landf. 37, 385–399.
Liebault, F., Lallias-Tacon, S., Cassel, M., Talaska, N., 2013. Long Profile responses of alpine braided rivers in SE France. River Res. Appl. 29, 1253–1266.
Liebault, F., Laronne, J.B., 2008. Evaluation of bedload yield in gravel-bed rivers using scour chains and painted tracers: the case of the Esconavette Torrent (Southern French Prealps). Geodin. Acta 21, 22–34.
Limaye, A.B., 2017. Extraction of multithread channel networks with a reduced-complexity flow model. J. Geophys. Res. Earth Surf. 122, 1972–1990.
Lotsari, E.S., et al., 2018. Topographical change caused by moderate and small floods in a gravel bed ephemeral river - a depth-averaged morphodynamic simulation approach. Earth Surf. Dyn. 6, 163–185.
Lu, X.X., Kummu, M., Oeurng, C., 2014. Reappraisal of sediment dynamics in the lower Mekong RiverCambodia. Earth Surf. Process. Landf. 39, 1855–1865.
Mahoney, J.M., Rood, S.B., 1998. Streamflow requirements for cottonwood seedling recruitment—an integrative model. Wetlands 18, 634–645.
Malard, F., 2003. Gorundwater-surface water interactions. In: Ward, J.V., Uehlinger, U. (Eds.), Ecology of a Glacial Floodplain. Kluwer, Dordrecht, pp. 37–56.
Malard, F., Uehlinger, U., Zah, R., Tockner, K., 2006. Flood-pulse and riverscape dynamics in a braided glacial river. Ecology 87, 704–716.
Marchetti, Z.Y., Minotti, P.G., Ramonell, C.G., Schivo, F., Kandus, P., 2016. NDVI patterns as indicator of morphodynamic activity in the middle Paraná River floodplain. Geomorphology 253, 146–158.
McCuen, R., 2004. Hydrologic Analysis and Design. Pearson Prentice Hall, Upper Saddle River, New Jersey.
Middleton, L., Ashmore, P., Leduc, P., Sjogren, D., 2019. Rates of planimetric change in a proglacial gravel- bed braided river: field measurement and physical modelling. Earth Surf. Process. Landf. 44, 752–765.
Misset, C., et al., 2020. Combining multi-physical measurements to quantify bedload transport and morphodynamics interactions in an Alpine braiding river reach. Geomorphology 351, 106877.
Nagler, P., Glenn, E.P., Hursh, K., Curtis, C., Huete, A., 2005. Vegetation mapping for change detection on an arid-zone river. Environ. Monit. Assess. 109, 255–274.
Naura, M., et al., 2016. Mapping habitat indices across river networks using spatial statistical modelling of River Habitat Survey data. Ecol. Indicat. 66, 20–29.
Ozyavuz, M., Bilgili, B.C., Salici, A., 2015. Determination of vegetation changes with NDVI method. J. Environ. Protect. Ecol. 16, 264–273.
Peirce, S., Ashmore, P., Leduc, P., 2018. The variability in the morphological active width: results from physical models of gravel-bed braided rivers. Earth Surf. Process. Landf. 43, 2371–2383.
Peixoto, J.M.A., Nelson, B.W., Wittmann, F., 2009. Spatial and temporal dynamics of river channel migration and vegetation in central amazonian white-water floodplains by remote-sensing techniques. Remote Sens. Environ. 113, 2258–2266.
Picco, L., et al., 2013. Evaluating short-term morphological changes in a gravel-bed braided river using terrestrial laser scanner. Geomorphology 201, 323–334.
Piégay, H., Alber, A., Slater, L., Bourdin, L., 2009. Census and typology of braided rivers in the French Alps. Aquat. Sci. 71, 371–388.
Powell, S.J., Jakeman, A., Croke, B., 2014. Can NDVI response indicate the effective flood extent in macrophyte dominated floodplain wetlands? Ecol. Indic. 45, 486–493.
Purevdorj, T.S., Tateishi, R., Ishiyama, T., Honda, Y., 1998. Relationships between percent vegetation cover and vegetation indices. Int. J. Remote Sens. 19, 3519–3535.
Raepple, B., Piégay, H., Stella, J.C., Mercier, D., 2017. What drives riparian vegetation encroachment in braided river channels at patch to reach scales? Insights from annual airborne surveys (Drôme River, SE France, 2005–2011). Ecohydrology 10 (8), e1886.
Redolfi, M., Tubino, M., Bertoldi, W., Brasington, J., 2016. Analysis of reach-scale elevation distribution in braided rivers: definition of a new morphologic indicator and estimation of mean quantities. Water Resour. Res. 52, 5951–5970.
Rouse, J.W., Haas, R.H., Shell, J.A., Deering, D.W., 1973. Monitoring Vegetation Systems in the Great Plains with ERTS, Third ERTS Symposium, NASA SP-351. In: NASA, Washington, DC, pp. 309–317.
Rozo, M.G., Nogueira, A.C.R., Castro, C.S., 2014. Remote sensing-based analysis of the planform changes in the Upper Amazon River over the period 1986–2006. J. S. Am. Earth Sci. 51, 28–44.
Sanhueza, D., et al., 2019. Quantification of fluvial wood using UAVs and structure from motion. Geomorphology 345.
Schwenk, J., Khandelwal, A., Fratkin, M., Kumar, V., Foufoula-Georgiou, E., 2017. High spatiotemporal resolution of river planform dynamics from Landsat: the RivMAP toolbox and results from the Ucayali River. Earth Space Sci. 4, 46–75.
Solari, L., Van Oorschot, M., Belletti, B., Vargas-Luna, A., 2015. Advances on modelling riparian vegetation—hydromorphology interactions. River Res. Appli. 32, 164–178.
Tal, M., Gran, K., Murray, B., Paola, C., Hicks, M., 2004. Riparian vegetation as primary control on channel characteristics in multi thread rivers. In: Bennett, S.J., Simon, A. (Eds.), Riparian Vegetation and Fluvial Geomorphology. Water Sci. Appl. Ser, AGU, Washington, D. C., pp. 43–58
Tamminga, A., Hugenholtz, C., Eaton, B., Lapointe, M., 2015. Hyperspatial remote sensing of channel reach morphology and hydraulic fish habitat using an unmanned aerial vehicle (UAV): a first assessment in the context of river research and management. River Res. Appl. 31, 379–391.
Tockner, K., Paetzold, A., Karaus, U., Claret, C., Zettel, J., 2006. Ecology of braided rivers. In: Sambrook Smith, G.H., Best, J.L., Bristow, C.S., Petts, G.E. (Eds.), aided Rivers: Process, Deposits, Ecology and Management. Special Publication. International Association of Sedimentologists, Kingston University, Surrey, pp. 339–359.
Torres-Sánchez, J., Peña, J.M., de Castro, A.I., López-Granados, F., 2014. Multi-temporal mapping of the vegetation fraction in early-season wheat fields using images from UAV. Comput Electron. Agric. 103, 104–113.
Tubino, M., Bertoldi, W., 2008. Bifurcations in gravel-bed streams. In: Habersack, H., Rinaldi, M., Pie'gay, H. (Eds.), Gravel-bed Rivers VI: From Process Understanding to River Restoration. Elsevier, Amsterdam, pp. 133–159.
Tucker, C.J., 1979. Red and photographic infrared linear combinations for monitoring vegetation. Remote Sens. Environ. 8, 27–150.
Ward, J.V., Tockner, K., Edwards, P.J., Kollmann, J., Bretschko, G., Gurnell, A.M., Petts, G.E., Rossaro, B., 1999. A reference river system for the Alps: the 'Fiume Tagliamenta'. Regulated Rivers: Res. Manag. 15 (3), 63–75.

Wawrzyniak, V., Piégay, H., Allemand, P., Vaudor, L., Grandjean, P., 2013. Prediction of water temperature heterogeneity of braided rivers using very high resolution thermal infrared (TIR) images. Int. J. Remote Sens. 34 (13), 4812–4831.
Werbylo, K.L., Farnsworth, J.M., Baasch, D.M., Farrell, P.D., 2017. Investigating the accuracy of photointerpreted unvegetated channel widths in a braided river system: a Platte River case study. Geomorphology 278, 163–170.
Williams, R.D., Brasington, J., Hicks, D.M., 2016. Numerical Modelling of Braided River Morphodynamics: Review and Future challenges. Geogr. Comp. 10, 102–127.
Williams, R.D., Rennie, C.D., Brasington, J., Hicks, D.M., Vericat, D., 2015. Linking the spatial distribution of bed load transport to morphological change during high-flow events in a shallow braided river. J. Geophys. Res. Earth Surf. 120, 604–622.
Xu, H., 2006. Modification of normalised difference water index (NDWI) to enhance open water features in remotely sensing imagery. Int. J. Remote Sens. 27, 3025–3033.
Zhou, W., Li, Z., Ji, S., Hua, C., Fan, W., 2015. A new index model NDVI-MNDWI for water object extraction in hybrid area. In: Bian, F., Xie, Y. (Eds.), Geo-informatics in Resource Management and Sustainable Ecosystem. Communications in Computer and Information Science, Springer, Berlin, Heidelberg, pp. 513–519.
Zolezzi, G., Bertoldi, W., Tubino, M., 2006. Morphological analysis and prediction of channel bifurcations. In: Sambrook Smith, G.H., Best, J.L., Bristow, C.S., Petts, G.E. (Eds.), Braided Rivers: Process, Deposits, Ecology and Management. International Association of Sedimentologists, Special Publication 36, Blackwell, Oxford, pp. 227–250.